Parameter Performance Analysis of Connection Nodes of T-Plate Connected Assembled Composite Shear Wall

Y Wang, Z Ma, S Qu*, J Zhao, P You

School of Civil and Transportation Engineering, Henan University of Urban Construction, Pingdingshan, 467036, China

ABSTRACT

With the development of construction industrialization, green and low-carbon construction methods have been strongly supported by domestic and foreign construction industries. As an efficient lateral force resistance system, the assembled steel plate-concrete composite shear wall structure has gradually become a hotspot in civil engineering. Referring to the node connection method of steel structure, this paper uses the concrete composite shear wall filled with steel plate and extended T-shaped gusset plate to realize the connection between the upper and lower walls, so as to form a T-plate connected assembled composite shear wall structure. Through establishing the refined finite element analysis model of cast-in-place and assembled composite shear wall with the same sizes and comparing the results of them, the feasibility and reliability of the connection method are verified. On this basis, according to the comparison between the bearing and continuity performance of the assembled composite shear wall under different parameters such as the T-plate length, T-plate flange width, T-plate number, joint height and joint longitudinal reinforcement ratio in the node connection area, it is found that the T-plate length, T-plate number and joint height have a great effect on the mechanical properties of assembled composite shear wall, and other parameters are not obvious. In this way, a reasonable recommendation is made for the connection parameters of T-node, which lays a theoretical foundation for promoting the theoretical development and engineering application of this new assembled composite shear wall.

1. INTRODUCTION

With the improvement of construction industrialization, the construction industry is in urgent need of transformation and upgrading. Traditional cast-in-place construction has gradually been replaced by more environmentally friendly and efficient assembled construction methods. The development of assembled buildings has received strong support from domestic and foreign policies. As an efficient lateral force resistance system, the assembled shear wall structure has become a new research hotspot in civil engineering. The node connection technology is the key to ensure the safety and reliability of assembled shear wall structure. For this reason, scholars have done a lot of research on the assembled shear wall structure using different node connection methods [1-6].

The common connection modes of existing assembled joints include sleeve grouting connection, grouting anchor lap connection, post-tensioned pre-stressed connection, keyway connection, wall Shoes connection and bolt connection [7-11].

*Corresponding Author: songgao241@163.com

Among them, the sleeve grouting connection and grouting anchor lap connection technology have developed rapidly [12-15]. This kind of connection method can effectively transfer the stress of reinforcement. The specimen failure mode of the assembled shear wall is basically the same as that of cast-in-situ shear wall. However, during on-site assembly, there are some problems such as difficult detection of embedded construction quality, difficulty in positioning the lap joint of the same cross-section and forced bending at construction site or violent construction behavior of cutting-off reinforcement. Moreover, when the wall is thin, it is easy to cause hole damage and affect the connection performance. Therefore, the application of the above connection methods in the development of assembled buildings is limited. Although post-tensioned pre-stressed connection has good self-resetting ability and energy dissipation effect [11], it has not attracted widespread attention due to the limitation of tensioning equipment and low redundancy of node connection. According to setting uniformly dense small keyways at the connection part, the keyway connection can ensure the uniformity of shear transmission and improve the reliability of node connection [16-18]. However, this setting will increase the size of keyway, and will affect the popularization and application of this connection. Comparing the Wall Shoes connection and the bolt connection [19-20], both of them are based on the wire drawing at the end of the threaded steel bar to form the screw end, and then cooperate with the nut or threaded sleeve to form an integral connection. They have extremely high requirements for the production and construction accuracy of the components. In addition, the precision requirements are extremely high and the stubble rebar is prone to bending and breaking, which will affect the assembly construction.

In order to overcome the shortcomings of traditional bolted connections based on steel wire drawing end connections, scholars began to focus on the connection using high-strength bolt and connecting steel frame [21-26]. There are connection forms represented by H-shaped steel frame, C-shaped steel frame, BPC structure and more. However, due to the complex and diverse forms of node connection steel frames and the large number of BPC connection bolts, the convenience, practicability and economy of node connection construction were affected to a certain extent. To this end, Huang g et al. directly spliced and connected the in-line steel plate connector and the embedded double steel plate in the wall [27], so as to avoid the adverse effects caused by the complex and diverse forms of connecting steel frames. The research has made some progress, but it does not give full play to the efficient and convenient characteristics of assembled buildings. Generally, the steel plate bolt joint connection has the advantages of high efficiency, convenience and reliable connection, and is especially suitable for assembled building structure system. In recent years, it has been widely recognized by domestic and foreign researchers.

In order to further improve the convenience of connection, reduce the use of connecting bolts and reduce the cost, the research group conducted a preliminary exploration on the fishplate connected assembled composite shear wall [28]. Based on the common bolted connection method of steel structures, this paper proposes a more secure and reliable T-plate connected assembled composite shear wall structure and conducts a series of tests on it to study the connection parameters of different nodes. The mechanical properties of the new assembled composite shear wall with different node connection parameters are studied, so as to lay a theoretical foundation for its application and development in engineering in the future.

2. DESIGN OF ASSEMBLED COMPOSITE SHEAR WALL

2.1 Connection node design

Fig.1 shows the joint structure of the T-plate connected assembled composite shear wall. The extended T-steel plate connectors are pre-embedded along the center line in the upper and lower edges of the precast wall.

During assembly, the lower edge of the upper wall is directly connected with the T-steel plate flanges protruding from the upper edge of the lower wall and fixed with bolts to complete the vertical connection of shear wall nodes. At the same time, the U-shaped stirrups are set at the gaps of T-steel plate connectors, which are bound with the longitudinal steel bars of the joints to form a dark beam bar cage, and then the concrete is poured to complete the assembly of the shear wall. Compared with the fishplate connection method [28], the flanges of T-steel plates are directly connected to each other. The force transmission is more reliable, and the vertical positioning devices such as spacers are not required, which can improve the connection efficiency and installation accuracy. The cross-shaped connection nodes formed by the combination of upper and lower T-steel plates after bolting have more reliable bending and shear resistance to ensure the safety of the assembled wall.

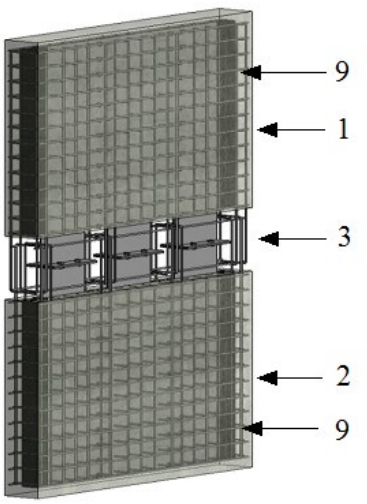

(a) Side view of connecting integral shaft

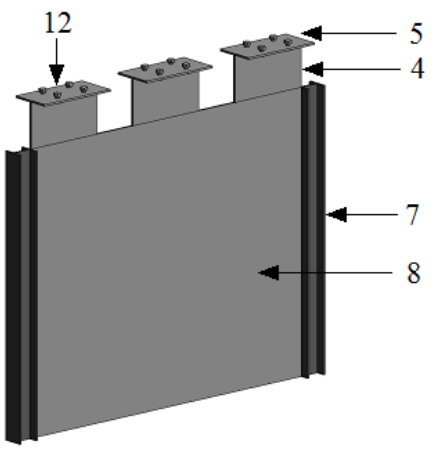

(b) Side view of internal steel plate shaft

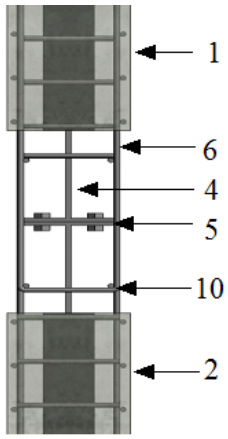

(c) Side view of connection node

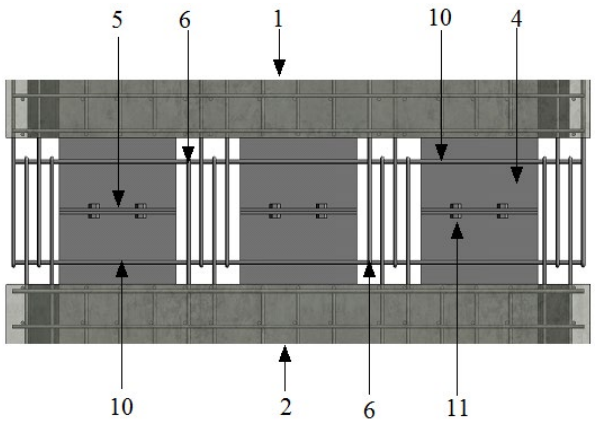

(d) Front view of connection node

Fig. 1: Structural drawing of bolted joints of T-plate. Note: 1-Precast upper wall; 2-Precast lower wall; 3- Node connection area; 4- Connector web of T-steel plate; 5- Connector flange of T-steel plate; 6- U-shaped stirrup bars; 7-Build-in I-beam; 8-Filled steel plate; 9-Distributed bars; 10- Joint longitudinal reinforcement; 11-Connecting bolt; 12- T-steel plate connector

2.2 Specimen design

The geometric dimension, internal reinforcement and internal steel plate of the cast-in-situ shear wall test model GB2-5-3 described in Zhu [29] are selected as the basic design parameters of the specimen, that is, except for the connection node area; the other parameters of the assembled composite shear wall are all consistent with the design parameters of GB2-5-3. The total wall is 1900 mm × 1000 mm × 120 mm; the loading beam is 1200 mm × 200 mm × 200 mm, and the ground beam is 1800 mm × 600 mm × 400 mm. The longitudinal and horizontal distribution bars are Φ6@80; the embedded column stirrups are Φ6@70, and the longitudinal bars of the embedded column are 4Φ10.

The longitudinal bars extend 180mm into the loading beam and 530mm into the ground beam. The diameter of U-shaped bar is 6mm; the spacing is 80mm, and the spacing between the horizontal distribution bars is 65mm. The thickness of the built-in steel plate in the wall is 5mm, and it extends 300mm into the ground beam and70mm into the loading beam. The T-shaped extended steel member is fully welded with the built-in steel plate, with a thickness of 5mm and a total height of 75mm. The profile steel column in the embedded column area is set as I54mm×50mm×5mm, and the profiled steel is 70mm deep into the loading beam and 530mm into the ground beam. Fig. 2 shows the schematic diagram of the reinforcing bars of the T-plate connected assembled composite shear wall.

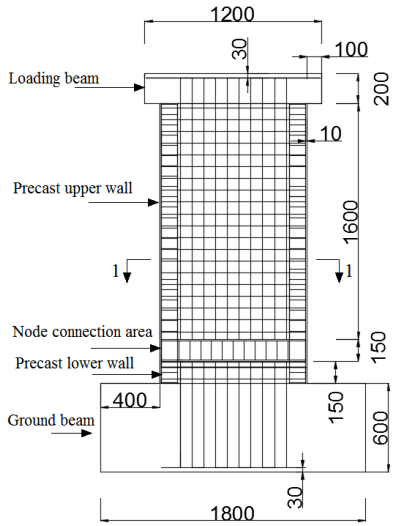

(a) Reinforcing bars of shear wall

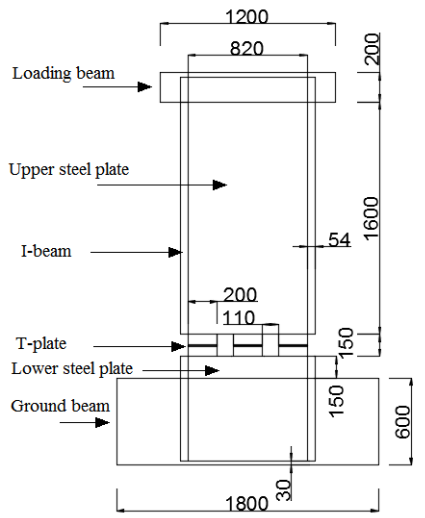

(b) Built-in steel plate of shear wall

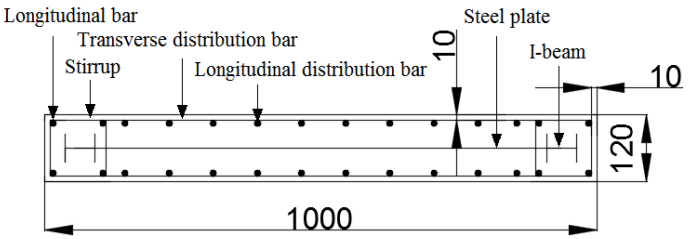

(c) 1-1 section

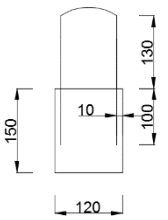

(d) U-shaped stirrup bars

Fig. 2: Schematic diagram of reinforcing bars of T-plate connected assembled composite shear wall (unit: mm)

In order to study the load bearing of T-plate connected assembled composite shear wall under different node connection parameters, the group tests were carried out and the specific parameters are shown in Table 1.

Table 1: Model number and parameter list

No.	L/**mm**	W/**mm**	**N**	H/**mm**	D/**mm**
XJ	—	—	—	—	—
TSP-CS	200	100	3	150	Φ6
TSP-L-1	100	100	3	150	Φ6
TSP-L-2	150	100	3	150	Φ6
TSP-W-1	200	60	3	150	Φ6
TSP-W-2	200	80	3	150	Φ6
TSP-N-1	200	100	2	150	Φ6
TSP-N-3	200	100	4	150	Φ6
TSP-H-2	200	100	3	200	Φ6
TSP-H-3	200	100	3	250	Φ6
TSP-D-0	200	100	3	150	—
TSP-D-2	200	100	3	150	Φ8
TSP-D-3	200	100	3	150	Φ10

Note: XJ is the cast-in-place shear wall model; "—" indicates that this parameter is not considered, and TSP stands for assembled shear wall model. Among them H, CS is the initial comparison model. L, W and N are the length, flange width and number of T-plates,

respectively. H is the height of the joint; D is the diameter of the longitudinal bar of the joint, and the numbers at the tail are the model numbers of different parameters. The modeling parameters of TSP-L-3, TSP-W-3, TSP-N-2, TSP-H-1 and TSP-D-1 are the same as those of the model TSP-CS, and they are not listed in the table.

3. BASIC PERFORMANCE ANALYSIS OF ASSEMBLED COMPOSITE SHEAR WALL

3.1 Finite element model establishment

(1) Element selection and grid size

In this paper, the finite element analysis software ABAQUS is used for structural modeling and analysis. The reinforcement element adopts the three-dimensional truss element two-node linear T3D2, and the concrete, embedded steel plate and bolt elements adopt the 8-node linear reduced integration C3D8R. Through the mesh convergence analysis, it is finally determined that the length of the concrete mesh and steel plate are set to 60 mm and 50 mm, respectively, and the mesh size of the loading beam is set to 100 mm.

(2) Material constitutive relation

ABAQUS finite element software provides a plastic damage model for simulating concrete cracking and crushing. The model has good convergence and can be applied to static and dynamic analysis. It can effectively simulate the inelastic properties of concrete under cyclic reciprocating loads. According to the test data of the specimen GB2-5-3, the strength parameters of concrete material are shown in Table 2. Combined with the "Code for Design of Concrete Structures" (GB50010-2010) [30], the uniaxial tension-compression constitutive relationship curve of concrete is calculated, as shown in Fig. 3.

The formula for calculating the uniaxial tensile stress and strain of concrete is shown as:

$$\sigma = (1 - d_t)E_c\varepsilon \tag{1}$$

The formula for calculating the uniaxial compressive stress and strain of concrete is shown as:

$$\sigma = (1 - d_c)E_c\varepsilon \tag{2}$$

where E_c is the elastic modulus of concrete; d_t and d_c are the uniaxial tensile and compressive damage evolution parameters of concrete, respectively. The selection method refers to "Code for Design of Concrete Structures".

Table 2 Main material parameters of concrete

$f_{cu,k}$/MPa	f_{ck}/MPa	f_{tk}/MPa	E_c/MPa	υ_c
82.37	58.58	3.85	38150	0.2

Note: $f_{cu,k}$ is the average cube compressive strength of concrete; f_{ck} is the standard value of concrete compressive strength; f_{tk} is the standard value of concrete tensile strength, and υ_c is the Poisson ratio of concrete.

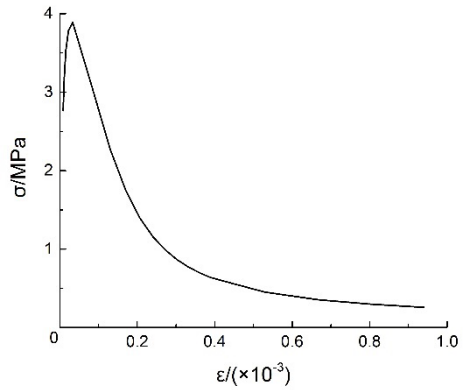

(a) Uniaxial tension

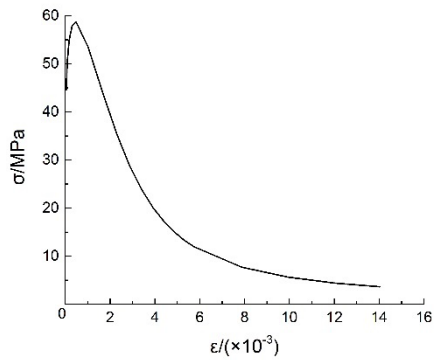

(b) Uniaxial compression

Fig. 3: Concrete constitutive relation curve

The elastic-plastic model in ABAQUS finite element software can be used to simulate the properties of steel. The constitutive relations of the high-strength bolts, steel bars and pre-embedded steel connection devices all adopt the ideal elastic-plastic model of the double-fold line, as shown in Fig. 4. According to the test data of the specimen GB2-5-3, combined with the "Code for Design of Steel Structures" (GB50017-2017) [31], the main parameters of the steel are shown in Table 3. Among them, the elastic modulus E_S in the linear elastic stage and the modulus $E'S$ in the strengthening stage are shown in formula (3) and formula (4), respectively:

$$E_S = tan\,\theta = \frac{f_y}{\varepsilon_s} \tag{3}$$

$$E_S^{'} = tan\,\theta^{'} = \frac{f_u - f_y}{\varepsilon_u - \varepsilon_s} \tag{4}$$

where f_y is the steel yield strength; f_u is the ultimate strength of steel; ε_s is the steel yield strain; ε_u is the ultimate strain of steel, and $E_S' = 0.01E_S$.

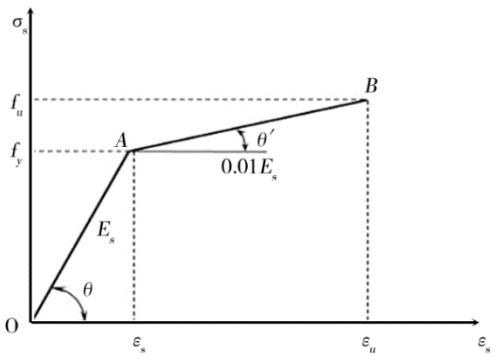

Fig. 4: Schematic diagram of steel constitutive relation curve

Table 3: Main material parameters of steel

Specification	f_y/**MPa**	f_u/**MPa**	E_S/**MPa**	$\boldsymbol{v_s}$
Φ6 bar	498	718	210000	0.3
Φ10 bar	475	694	200000	0.3
Steel plate	353	460	206000	0.3
M16-10.9S	846	941	210000	0.3

(3) Boundary conditions

Considering that the built-in steel plate of the composite shear wall is constrained by the surrounding concrete, ignoring the bond slip between the steel and concrete, the steel is built into the concrete. At the same time, the bond slip between the bolt and T-shaped connection plate is ignored. The contact surfaces of the upper and lower T-plate flanges are set as contact elements. Consistent with the test boundary conditions, the ground beam is set to be consolidated and the loading beam is set to be a sliding bearing along the in-plane direction of the wall.

(4) Loading method

In the finite element solution, two-step loading is used. The first step is vertical loading. The axial pressure is applied to ensure that the loading beam is evenly stressed to avoid stress concentration. A reference point is established at the midpoint of the top surface of the loading beam and coupled with the top surface of the loading beam. Axial pressure is applied through the reference point and remains constant throughout the solution. The second step is horizontal loading. The action point is located on the cross section of the end of the loading beam; the low-cycle reciprocating horizontal thrust is applied, and the loading is controlled by displacement until the specimen yields the failure. According to the above parameter settings, the finite element models of the cast-in-situ and assembled composite shear walls are established respectively, as shown in Fig. 5.

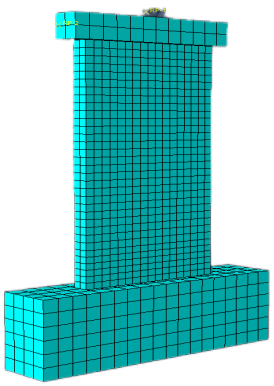

(a) Cast-in-situ shear wall model

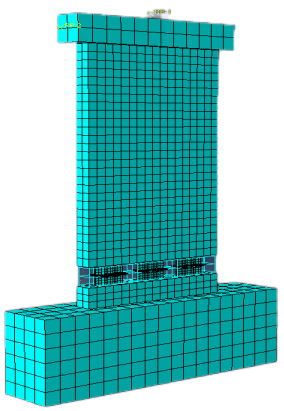

(b) Assembled Shear Wall Model

Fig. 5: Schematic diagram of the finite element model

3.2. Model test

In order to verify the rationality of the finite element model, the finite element analysis models corresponding to the specimen GB2-5-3 and GB2-3-3 in Zhu [29] were established according to the above modeling methods, and the loading test was carried out. The loading regime is consistent with the test process. The first step is to apply vertical pressure to the top of the loading beam to 2700KN and 2230KN, respectively, and the test axial pressure ratio is 0.30. The second step is to apply a low cycle reciprocating horizontal thrust at the end of the loading beam, using displacement for control. A reciprocating load at a displacement of 2 mm per stage is applied until the specimen fails. The finite element analysis is compared with the results obtained from the test, and the results are shown in Fig. 6 and Table 4. The error calculation is as follows:

$$E_{rror} = \frac{S_{value} - E_{value}}{E_{value}} \times 100\% \tag{5}$$

where $Error$ is the calculation error; S_{value} and E_{value} are the finite element analysis and experimental values, respectively.

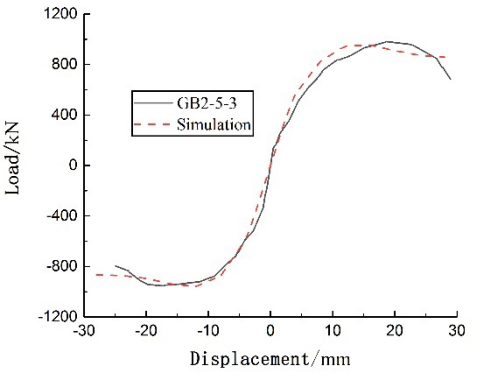

(a) Specimen GB2-5-3

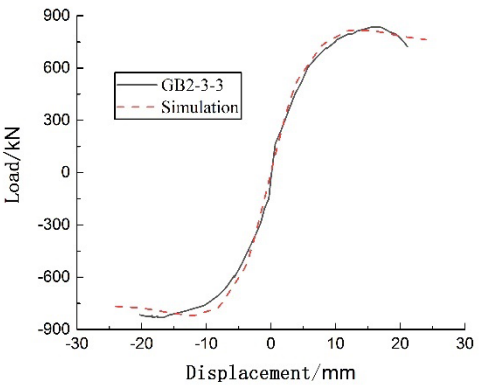

(b) Specimen GB2-3-3

Fig. 6 Comparison of skeleton curve between finite element analysis and test values

It can be seen from Fig. 6(a) and Fig. 6 (b) that the test curve and skeleton curve obtained by the finite element analysis are basically consistent. At the initial stage of loading, the slope of them is basically constant. This shows that the lateral stiffness of the specimen is basically unchanged at this stage. With the increase of the load, the slopes of the two skeleton curves gradually decrease, and the shear stiffness of the specimen gradually weakens. At the same time, the peak load Pmax obtained by the finite element analysis is very close to the experimental value. As shown in Table 4, the calculation error of the two groups of tests is less than 3%, and the finite element calculation results are in good agreement with the test results. In this way, the finite element analysis model established by ABAQUS, and the setting of modeling parameters has good feasibility and accuracy.

Table 4: Comparison between finite element analysis and test peak load

No.	P_{max}/kN		Error/%
	E_{value}	S_{value}	
GB2-5-3	963	954	-0.93
GB2-3-3	822	806	-1.95

3.3. Basic performance analysis

According to the above finite element modeling method and referring to the size and material properties of model GB2-5-3, the initial model TSP-CS for T-plate connected assembled composite shear wall and the analysis model XJ for cast-in-situ composite shear wall are established, and the finite element analysis is carried out. The comparison between the hysteresis curve and the skeleton curve of them is shown in Fig. 7 and Fig. 8.

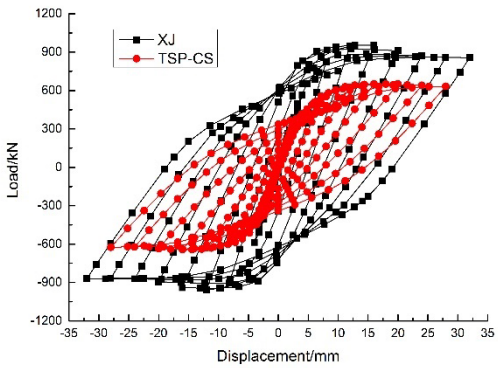

Fig. 7: Hysteretic curve comparison

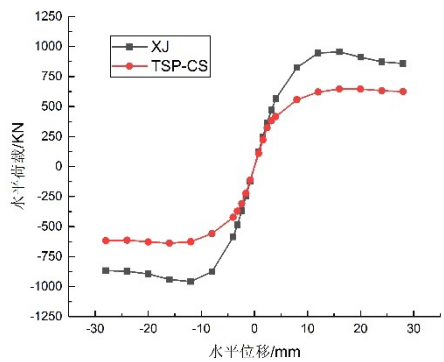

Fig. 8: Skeleton curve comparison

It can be seen from Fig. 7 that the hysteresis curves of TSP-CS and XJ are both shuttle-shaped, indicating that both have optimal plastic deformation ability, seismic performance and energy dissipation capacity. In contrast, the hysteretic curve of XJ is fuller, and that of TSP-CS is slightly pinched. The hysteretic loop area of the latter is smaller than that of the former. This indicates that there is a slip phenomenon in the joint connection area of the assembled composite shear wall, resulting in the decline of its energy dissipation capacity.

It can be seen from Fig. 8 that the skeleton curves of XJ and TSP-CS are basically the same, and both show an inverse "Z" shape, which can be roughly divided into the linear elastic stage, the elastic-plastic stage and the failure stage. In the linear elastic stage, concrete, steel bars and steel plates work together to bear the action of horizontal load. This stage presents a straight-line segment with a constant slope. In the elastic-plastic stage, due to the generation of concrete cracks, most of the force is borne by the steel bar and steel plate, and the two curves both form a curve segment with a decreasing slope. In the failure stage, as the load increases, the concrete at the compression edge of the shear wall is crushed, and the restraint of steel plate is lost. After reaching the peak load, the skeleton curves of XJ and TSP-CS both show a descending segment. Meanwhile, the peak load of TSP-CS is less than that of XJ. The main reason is that after entering the elastic-plastic stage, the load of the built-in steel plate gradually increases. Due to the discontinuity of T-gusset plate at the horizontal joint, the sum of the lengths of T-shaped gusset plates at the joint of the new assembled composite shear wall is far less than that of built-in steel plate of cast-in-situ shear wall, resulting in a decrease in the bearing of assembled composite shear wall in the elastic-plastic stage.

Therefore, the change trend of load displacement curve of T-plate connected assembled composite shear wall and cast-in-situ composite shear wall is basically the same. This indicates that the failure mode of assembled composite shear wall is similar to that of cast-in-situ composite shear wall, and it is an effective and feasible node connection mode of assembled shear wall.

4. PARAMETER OPTIMIZATION ANALYSIS OF ASSEMBLED COMPOSITE SHEAR WALL

The following will focus on the difference of connection parameters in the node area, and discuss the change law of the mechanical properties of the new assembled composite shear wall, so as to recommend safer and more reliable node connection parameters.

4.1. T-plate length

In order to analyze the influence of T-steel plate length on the bearing performance of the wall, the finite element analysis models TSP-L-1, TSP-L-2 and TSP-L-3 with the length of T-steel plate of 100mm, 150mm and 200mm were established, respectively. The detailed parameters are shown in Table 1. The modeling method and loading process are the same as those described in Section 2 and Section 3.

The ductility is an important parameter index of the shear wall structure, which reflects the overall plastic deformation ability of the structure. In order to quantitatively evaluate the influence of T-steel plate length on the mechanical properties of assembled composite shear wall specimens, the ductility coefficient μ can be used to quantitatively describe as (the same below will not be repeated),

$$\mu = \frac{\Delta_u}{\Delta_y} \tag{6}$$

where Δu is the limit displacement and Δy is the yield displacement.

In this paper, the Park method is used to determine the yield displacement. The ultimate displacement is the corresponding displacement point when the bearing capacity drops to 85% of the peak load. If the load-displacement curve does not decrease, the limit displacement is the maximum horizontal displacement reached by the last loading. As a result, the skeleton curve and ductility coefficient of the specimen under the condition of different T-steel plate lengths are obtained as shown in Fig. 9 and Table 5.

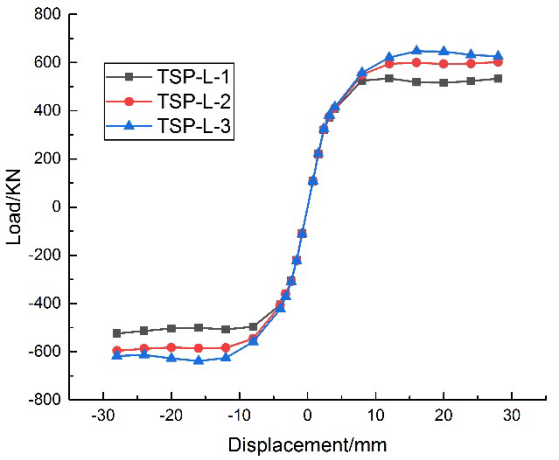

Fig. 9: Skeleton curves under different lengths of T-steel plates

It can be seen from Fig. 9 that the assembled composite shear wall has reliable bearing performance under the three lengths of T-steel plates. In the linear elastic stage, the skeleton curves of the three almost completely overlap. After entering the elastic-plastic stage, the skeleton curves of them begin to separate. With the increase of the T-steel plate length, the bearing performance of assembled composite shear wall is gradually increasing, and the peak load of TSP-L-3 is the largest.

Table 5: Bearing capacity and ductility coefficient under different lengths of T-steel plates

No.	L**/mm**	P_y**/kN**	Δ_y**/mm**	P_{max}**/kN**	Δ_u**/mm**	μ
TSP-L-1	100	440.61	5.13	534.33	28	5.45
TSP-L-2	150	511.07	6.90	601.53	28	4.05
TSP-L-3	200	555.24	7.94	646.84	28	3.53

Table 5 gives the bearing capacity and ductility coefficient of the assembled composite shear walls with different lengths of T-steel plates. It is found that the ductility coefficients of the three T-steel plate lengths are all more than 3.0, which meets the seismic requirements. However, with the increase of T-steel plate length, the ductility coefficient gradually decreases, indicating that the ductility performance of the assembled composite shear wall has a downward trend. Meanwhile, with the increase of the T-steel plate length, the yield load and peak load of the assembled composite shear wall gradually increases, and the bearing performance continued to improve.

Generally, the length of T-steel plate has a significant impact on the bearing and ductility of the assembled composite shear wall. The length should be appropriately increased to improve its seismic bearing capacity under the condition that the ductility index requirements are met.

4.2. T-plate flange width

In order to analyze the influence of the T-plate flange width of the node on the bearing performance of the wall, the finite element analysis models TSP-W-1, TSP-W-2 and TSP-W-1, TSP-W-2 and TSP- W-3 with the T-shaped plate flange width of 60mm, 80mm and 100mm are established, respectively. The nonlinear finite element analysis is carried out to obtain the skeleton curve and ductility coefficient under different T-plate flange widths, as shown in Fig.10 and Table 6.

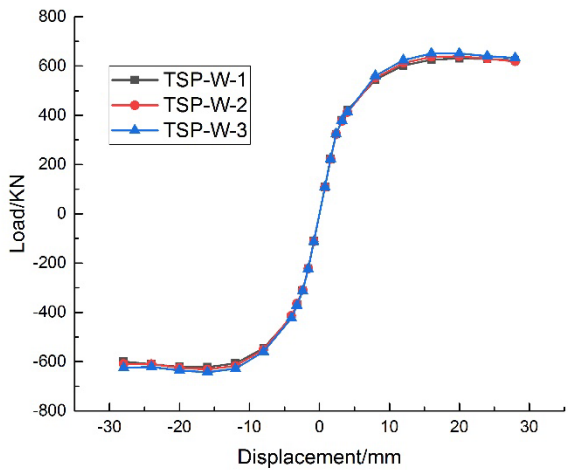

Fig. 10: Skeleton curves under different T-plate flange widths

Table 6: Bearing capacity and ductility coefficient of different T-plate flange widths

No.	W**/mm**	P_y**/kN**	Δ_y**/mm**	P_{max}**/kN**	Δ_u**/mm**	μ
TSP-W-1	60	531.74	7.61	630.72	28	3.68
TSP-W-2	80	548.52	7.92	639.49	28	3.53
TSP-W-3	100	555.24	7.94	646.84	28	3.53

It can be seen from Fig.10 and Table 6 that different T-plate flange widths have little effect on the bearing and ductility of the assembled composite shear wall. In the case of three T-plate flange widths, the skeleton curves of the assembled composite shear wall are basically coincident. Meanwhile, the yield load, yield displacement and peak load of them are not much different, and the ductility coefficients are all around 3.6, with little change. Thus the T-slab

flange width has little effect on the bearing and ductility of the assembled composite shear wall, and the T-plate flange width can be appropriately reduced if the construction requirements are met.

4.3. Number of T-plates

In order to analyze the influence of T-plates on the bearing performance of the wall, the finite element analysis models TSP-N-1, TSP-N-2 and TSP-N-3 with 2, 3 and 4 T-plate connections are established, respectively, and the nonlinear finite element analysis is carried out. The skeleton curve and ductility coefficient under different number of T-plates are obtained, as shown in Fig. 11 and Table 7.

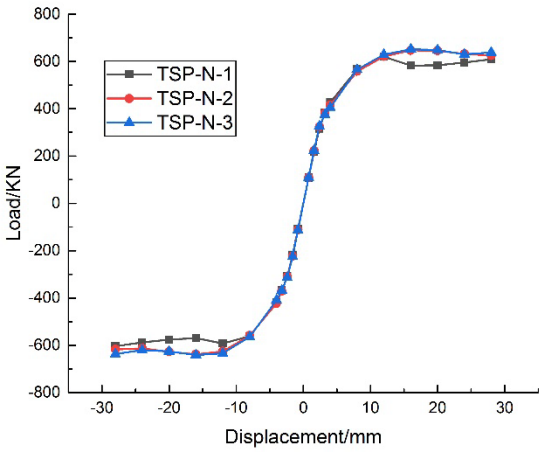

Fig.11: Skeleton curve under different number of T-plates

Table 7: Bearing capacity and ductility coefficient under different number of T-plates

No.	N	P_y/kN	Δ_y/mm	P_{max}/kN	Δ_u/mm	μ
TSP-N-1	2	523.58	6.78	619.64	28	4.42
TSP-N-2	3	555.24	7.94	646.84	28	3.53
TSP-N-3	4	567.30	8.12	652.07	28	3.45

Comparing the skeleton curves of assembled composite shear wall with three numbers of T- plates in Fig. 11, it is found that the three curves are in good agreement in the online elastic stage and the elastic-plastic stage. After the wall bearing capacity reaches the peak load in the failure stage, the bearing of model TSP-N-1 decreases rapidly, while that of TSP-N-2 and TSP-N-3 are still very close. Therefore, in the failure stage, because the bearing capacity of the node connection area is mainly borne by the steel plate, when the joint is connected with two T-plates, the node connection area is more prone to relative slip. The wall stiffness decreases rapidly, and the bearing performance is not easy to be guaranteed.

It can be seen from Table 7 that with the decrease of T-plates, the yield load and peak load of the wall both decrease continuously, while the ductility coefficient increases. The peak load and ductility coefficient of TSP-N-2 and TSP-N-3 are relatively close. The ductility coefficient of TSP-N-1 increases and the peak load of it decreases significantly.

Generally, the number of T-plates in the node connection area has a certain effect on the bearing and ductility of the assembled composite shear wall. In order to ensure the safety and reliability of the assembled composite shear wall, the T-plates in the node connection area should not be less than 2.

4.4. Joint height

In order to analyze the effect of joint height on the bearing performance of wall, the finite element analysis models TSP-H-1, TSP-H-2 and TSP-H-3 with the joint heights of 150mm, 200mm and 250mm are established. After analysis, the skeleton curve and ductility coefficient under different joint heights are shown in Fig. 12 and Table 8.

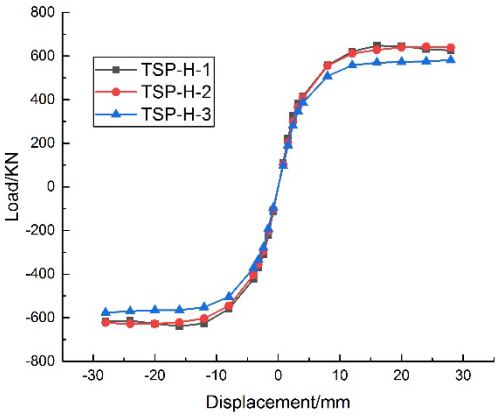

Fig. 12: Skeleton curves under different joint heights

Table 8: Bearing capacity and ductility coefficient under different joint heights

No.	H**/mm**	P_y**/kN**	Δ_y**/mm**	P_{max}**/kN**	Δ_u**/mm**	μ
TSP-H-1	150	555.24	7.94	646.84	28	3.53
TSP-H-2	200	555.64	8.04	643.48	28	3.48
TSP-H-3	250	492.75	7.50	581.26	28	3.73

It can be seen from Fig. 12 and Table 8 that the joint height has a certain effect on the bearing capacity and ductility of the assembled composite shear wall. With the increase of the joint height, the peak load of the assembled composite shear wall is downward. The ductility coefficient changes, but the change range is not obvious. Among them, when the joint height does not exceed 200mm, the yield load, peak load and ductility coefficient of TSP-H-1 and TSP-H-2 are relatively close, while that of TSP-H-3 decrease greatly. Generally, the joint height of the assembled composite shear wall should not be too large, and the minimum joint height to meet the construction requirements is appropriate.

4.5. Longitudinal reinforcing ratio of joint

In order to analyze the influence of the longitudinal reinforcement ratio in the node connection area on the bearing performance of the wall, the model TSP-D-0 without joint longitudinal reinforcement and the models TSP-D-1, TSP-D-2 and TSP-D-3 with joint longitudinal

reinforcement at the diameters of 6 mm, 8 mm and 10 mm are established, and the nonlinear finite element analysis is carried out. The skeleton curve and ductility coefficient under different reinforcement ratios are obtained as shown in Fig.13 and Table 9, respectively. The formula for calculating the joint longitudinal reinforcement ratio ρ is shown as,

$$\rho = \frac{A_{bar}}{B \times H} \times 100\% \tag{7}$$

where A_{bar} is the area of all longitudinal reinforcement at the joint; B is the thickness of shear wall, and H is the joint height.

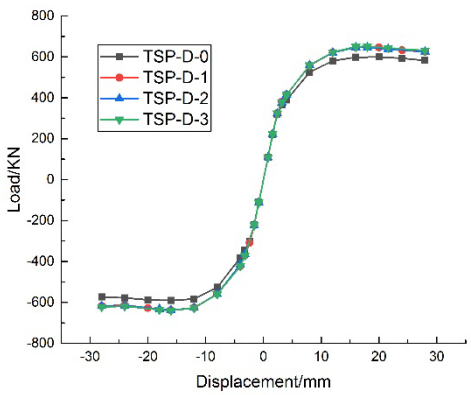

Fig. 13: Skeleton curve under different joint reinforcement ratios

Table 9: Bearing capacity and ductility coefficient under different joint reinforcement ratios

No.	ρ/**%**	P_y/**kN**	Δ_y/**mm**	P_{max}/**kN**	Δ_u/**mm**	μ
TSP-D-0	0	514.72	7.71	599.02	28	3.60
TSP-D-1	0.63	555.24	7.94	646.84	28	3.53
TSP-D-2	1.12	556.90	7.93	646.73	28	3.53
TSP-D-3	1.74	560.17	8.03	650.67	28	3.48

It can be seen from Fig.13 and Table 9 that the skeleton curves of the three models with longitudinal reinforcement in the node area are basically coincide. The yield load and peak load are close, and the ductility coefficients are basically the same, indicating that the level of the joint longitudinal reinforcement ratio has little effect on the bearing and ductility of the wall. Comparing the skeleton curve of TSP-D-0 and the model with joint longitudinal reinforcement, it is found that the yield load and peak load of TSP-D-0 decrease, and the ductility coefficient increases with little change.

It can be seen that longitudinal reinforcement ratio of the joint is not a key factor affecting the bearing performance of the wall, but in order to ensure the integrity and rigidity of the wall connection, an appropriate amount of longitudinal reinforcement should be arranged in the joint connection area.

5. CONCLUSION

In this paper, a T-plate connected assembled composite shear wall structure is proposed, and finite element modeling and analysis are carried out to verify the feasibility of the new node connection method. On this basis, a series of comparative experimental studies are carried out on the parameters of the T-plate length, T-plate flange width, T-plate number, joint height and joint longitudinal reinforcement ratio in the node connection area. On the premise of ensuring the reliable bearing and good continuation performance of the assembled composite shear wall, a rational recommendation is made for the selection of the above parameters. The main research conclusions are as follows:

1) The T-plate connected assembled composite shear wall has reliable bearing and good continuation performance, and the T-plate bolt connection is a safe and feasible node connection method.
2) The failure mode of the assembled composite shear wall is similar to that of the cast-in-situ composite shear wall, but the new assembled composite shear wall has lower energy dissipation capacity and bearing capacity.
3) The length and number of T-shaped plates have a great impact on the bearing and ductility of the wall. On the premise of meeting the ductility performance, the length and number of T-shaped plates should be appropriately increased to improve the seismic bearing capacity of the wall.
4) The flange width and joint longitudinal reinforcement ratio of T-plate have little effect on the bearing performance and ductility of the wall. When selecting the node parameters, the structural reinforcement ratio that meets the minimum flange width required for construction and the design requirements shall prevail.
5) The joint height will have a certain impact on the bearing performance of the assembled composite shear wall. In order to ensure the bearing capacity of the wall, the joint height should not be too high, and the minimum joint height meeting the construction requirements is appropriate.

The assembled composite shear wall with T-plate connection has optimal applicability and development prospects, and it is a practical method for the connection of assembled shear walls. However, compared with the cast-in-situ structure, it still has the disadvantage of insufficient bearing capacity. In order to further reveal the bearing law and failure characteristics of the new assembled composite shear wall and identify the key factors to improve its seismic bearing capacity, the optimization of connection node parameters and the real model test will become the focus of the next research work.

ACKNOWLEDGEMENT

The work was supported by the National Natural Science Foundation of China-Youth Science Fund (52108207), Key Scientific Research Projects of Colleges and Universities in Henan Province (22A560001) and Henan Science and Technology Research Project (212102310933).

REFERENCES

[1] Huang, W., Sun, Y.J., Zhang, J.R., Fan, Z.H., Ma, X., Research status of new connection technology of prefabricated wall structures. Industrial Construction, 2020, 50(7): p. 181-189.

[2] Kurama, Y.C., Sritharan, S., Fleischman, R.B., Restrepo, J.I., Henry, R.S., Cleland, N.M., Ghosh, S.K., Bonelli, P., Seismic-resistant precast concrete structures: state of the art. Journal of Structural Engineering, 2018, 144(4): p. 03118001.

[3] Losch, E.D., Hynes, P.W., Andrews Jr, R., Browning, R., Cardone, P., Devalapura, R., Yan, L., State of the art of precast/prestressed concrete sandwich wall panels. PCI Journal, 2011, 56(2): p. 131-176.

[4] Precast / Prestressed Concrete Institute (PCI). PCI design handbook: precast and prestressed concrete [M]. Chicago: The Donohue Group, Inc. 2017.

[5] Ye, J.H., Jiang, L.Q., Simplified analytical model and shaking table test validation for seismic analysis of mid-rise cold-formed steel composite shear wall building. Sustainability, 2018, 10(9): p. 3188.

[6] Lacey, A.W., Chen, W.S., Hao, H., Bi, K.M., Effect of inter-module connection stiffness on structural response of a modular steel building subjected to wind and earthquake load. Engineering Structures, 2020, 213: p. 110628.

[7] Ye, M., Qian, G.L., Hao, Z.Q., et al., Construction technology of steel bar sleeve grouting connection. Beijing: China Architecture Publishing& Media Co. Ltd. 2017.

[8] El Semelawy, M., El Damatty, A., Soliman, A.M., Finite-element analysis of anchor-jointed precast structural wall system. Structures and Buildings, 2017, 170(8): p. 543-554.

[9] Guo, T., Wang, L., Xu, Z.K., Hao, Y.W., Experimental and numerical investigation of jointed self-centering concrete walls with friction connectors. Engineering Structures, 2018, 161: p. 192-206.

[10] Psycharis, I.N., Kalyviotis, I.M., Mouzakis, H.P., Experimental investigation of the response of precast concrete cladding panels with integrated connections under monotonic and cyclic loading. Engineering Structures, 2018, 159: p. 75-88.

[11] Kurama, Y.C., Seismic design of partially post-tensioned precast concrete walls. PCI Journal, 2005, 50(4): p. 100-125.

[12] Belleri, A., Riva, P., Seismic performance and retrofit of precast concrete grouted sleeve connections. PCI Journal, 2012, 57(1): p. 97-109.

[13] Qian, J.R., Han, W.L., Zhao, Z.Z., Qin, Y., Zhang, Y., Yu, J., Ma, T., Tian, D., "Pseudo-dynamic substructure test on a 3-story full-scale model of prefabricated concrete shear wall structure with rebars splicing by grout sleeves. Journal of Building Structures, 2017, 38(3): p. 26-38.

[14] Zhang, W.Y., Yang, L.P., Yu, S.L., Zhang, Q.L., Cui, J.C., Research on key issues of the double-superimposed shear wall: experimental study on seismic performance of horizontal connections. China Civil Engineering Journal, 2018, 51(12): p. 28-41.

[15] Zang, X.L., Zhu, Z.F., Pseudo-static test on precast concrete shear walls with spiral stirrups-constraint bellows grouted connection. Construction Technology, 2018, 47(21): p. 82-87.

[16] Chang, Y.J., Liu, B.K., Song, G.H., Experimental study of force-bearing property of precast reinforced concrete assemblage (PRCA) with vertical joint composed of dowel and alveolus connection under low-cyclic-repeated loading. Industrial Construction, 2001, 31(9): p. 30-32+68.

[17] Zhang, X.Z., Li, J.W., Li, F.L., Dou, Y.B., Guo, H.Y., Li, Y.N., Effect of joint treatment on the seismic performance of prefabricated shear wall with composite alveolar. Journal of Tianjin University (Science and Technology), 2021, 54(6): p. 575-584.

[18] Chen, W., Wu, Q., Wu, D.Y., Wang, S.L., Guo, Z.X., Jiang, F.F., Mechanical behavior of new precast shear walls with reinforced tenon by numerical simulation and theoretical analysis. Concrete, 2020, (12): p. 50-55.

[19] Peikko Group. PSK Wall Shoe[R]. Peikko News, 2006.

[20] Lim, W.Y., Kang, T.H.K., Hong, S.G., Cyclic lateral testing of precast concrete t-walls in fast low-rise construction. ACI Structural Journal, 2016, 113(1): p. 179-189.

[21] Chen, Z.H., Liu, J.D., Yu, Y.J., Experimental study on interior connections in modular steel buildings. Engineering Structures, 2017, 147: p. 625-638.

[22] Guo, W., Zhai, Z.P., Cui, Y., Yu, Z.W., Wu, X.L., Seismic performance assessment of low-rise precast wall panel structure with bolt connections. Engineering Structures, 2019, 181: p. 562-578.

[23] Jiang, J.L., Han, J., Ren, W., Li, Y.M., Study on bearing capacity and seismic properties of prefabricated skip-floor shear walls with bolted connection. Industrial Construction, 2021, 51(1): p. 45-53+109.

[24] Sun, J., Qiu, H.X., Xu, J.P., Experimental and theoretical study on shear capacity of vertical joints in IPSW system. Journal of Southeast University (Natural Science Edition), 2014, 44(3): p. 631-637.

[25] Gao, X.J., Seismic Behavior Research of Precast Reinforced Concrete Shear Wall with Bolted Steel Plate Joints. Beijing: Beijing University of Civil Engineering and Architecture, 2019.

[26] Zhu X.Z., Total bolt connection prefabricated concrete structure joints and carrying capacity research. Wuhan: Wuhan University of Technology. 2017.

[27] Huang, S.T., Huang, Y.S., Cai, J., Tang, X.L., Zuo, Z.L., Seismic behavior test of steel-concrete-steel composite shear wall with vertical seams and horizontal bolt connections. Journal of Building Structures, 2021, 42(7): p. 164-172.

[28] Wang, Y., Wang, Z.C., Zhao, J., Qu, S.Z., Analysis on Mechanical Properties of Prefabricated Composite Shear Wall Connected with Fish Plate. Journal of Three Gorges University (Natural Science), 2021, 43(3): p. 47-53.

[29] Zhu, A.P., Seismic performance of built-in steel plate-C80 concrete composite shear wall. Beijing: China Academy of Building Research. 2015

[30] GB50010-2010. Code for design of concrete structures. China Architecture & Building Press, 2015.

[31] GB50017-2017. Code for design of steel structures. China Architecture & Building Press, 2017.